Available online at www.sciencedirect.com
SCIENCE DIRECT®
Physics of the Earth and Planetary Interiors 148 (2005) 233–250
PHYSICS OF THE EARTH AND PLANETARY INTERIORS
www.elsevier.com/locate/pepi

Seismic discontinuities in the Mediterranean mantle

M. van der Meijde*, S. van der Lee[1], D. Giardini

Institute of Geophysics, Swiss Federal Institute of Technology, CH-8093 Zurich, Switzerland

Received 28 July 2003; received in revised form 8 August 2004; accepted 3 September 2004

Abstract

Layering in the upper and lower mantle across the Mediterranean has been determined using *P*-to-*S* converted phases identified through receiver function analysis. Conversion of the receiver function's time axis to depth was based on local 1D *S*-velocity models. The 1D velocity model for each station was extracted from a three-dimensional *S*-velocity model for the Mediterranean region (EAV03), enhanced with crustal structure derived from receiver function analysis. Under the Mediterranean region we observed a mantle transition zone thickness of 261 ± 10 km, on average, which agrees with a dominance of high velocities imaged in tomographic models at these depths. A thick mantle transition zone (>270 km) was observed in regions with ongoing or past subduction: eastern Spain, southern Italy, southern Greece and the north-western African coast. Conversions from the 410 km and 660 km discontinuities were clearly observed for most stations. Amplitudes of both discontinuities are anomalously large throughout the Mediterranean region, 4.9% and 5.7%, respectively. We observed significant conversions from the 520 km discontinuity. The lower mantle showed strong lateral variations resulting in spatially incoherent converted phases from discontinuities near 860 km, between 900 km and 1200 km, and 1320 km depth.

Keywords: Discontinuities; Upper mantle; Lower mantle; Transition zone; Receiver functions; Mediterranean

1. Introduction

Global 1D Earth models (Kennett et al., 1995; Morelli and Dziewonski, 1993; Kennett and Engdahl, 1991; Dziewonski and Anderson, 1981) show two major discontinuities in the mantle, one around 410 km and one near 660 km depth (hereafter referred to as *d*410 and *d*660). These discontinuities border the mantle transition zone. An additional discontinuity, although not present in global models, is often reported around 520 km depth (hereafter referred to as *d*520). The results of high pressure and temperature laboratory experiments (Ito and Takahashi, 1989; Katsura and Ito, 1989; Ringwood, 1975) suggest that the mantle transition zone discontinuities may be caused by phase changes in olivine. These major upper mantle phase transitions involve the one from

* Corresponding author. Present address: International Institute for Geo-information Science and Earth Observation (ITC), P.O. Box 6, 7500 AA, Enschede, The Netherlands.
E-mail address: vandermeijde@itc.nl (M. van der Meijde).
[1] Present address: Department of Geological Sciences, 306 Locy Hall, 1850 Campus Drive, Northwestern University, Evanston, IL 60208-2150, USA.

0031-9201/$ – see front matter © 2004 Elsevier B.V. All rights reserved.
doi:10.1016/j.pepi.2004.09.008

olivine to wadsleyite at the *d*410, wadsleyite to ringwoodite around 520 km and ringwoodite to perovskite and magnesiowüstite at the *d*660 (Helffrich, 2000). These discontinuities are characterized by a jump in *P*-wave and *S*-wave velocity and density. These jumps are 1.7 ± 0.3 times larger for the *d*660 than for the *d*410 in the aforementioned global 1D earth models (Kennett et al., 1995; Morelli and Dziewonski, 1993; Kennett and Engdahl, 1991; Dziewonski and Anderson, 1981). Recent seismic observations (Helffrich et al., 2003; Shearer and Flanagan, 1999) find comparable jumps in both velocities and density for the *d*660 and *d*410 whereas others find a much weaker *P*-wave contrast from *PP*-precursors originating from the d660 *d*660 (Estabrook and Kind, 1996). Estimates for the velocity jump at the *d*520 varies between seven times weaker than for the *d*660 (Rigden et al., 1991) up to comparable to that for the *d*660 (Inoue et al., 1998), with intermediate estimates from seismic observations (Shearer, 1991; Revenaugh and Jordan, 1991; Revenaugh, 1990).

Although they are called the 410-km and 660-km discontinuity their actual depths may differ from these values. In global *SS*-precursor studies the *d*410 and *d*660 are found at average depths of 418 km and 660 km, respectively (Flanagan and Shearer, 1998). The reported maximum depth variation of the discontinuities depends strongly on the type of study. Short-period receiver function studies (Collier and Helffrich, 1997; Niu and Kawakatsu, 1995; Vidale and Benz, 1992; Richards and Wicks, 1990), report larger topography (30–70 km) than *SS*-precursor studies (10–20 km) (Gu and Dziewonski, 2002; Flanagan and Shearer, 1998; Shearer, 1991). *SS*-precursor studies sample larger regions around the point of investigation (2000 km compared to 200 km or less for the previous called short-period studies) leading to inaccuracy in the topography estimates (Neele et al., 1997). The phase changes responsible for the *d*410 and *d*520 have positive pressure-temperature gradients (Clapeyron slope), 3.1 and 5.3 MPa K^{-1} (Helffrich, 2000), respectively, so that a rise in temperature results in an increase in pressure (depth) of the phase change. For the phase change responsible for the *d*660 the Clapeyron slope is negative (-2.0 MPa K^{-1} (Bina and Helffrich, 1994)) so that a rise in temperature will lead to a decrease in the pressure (depth). This implies an anti-correlation between the *d*410 and the *d*660: where one of the discontinuities is bent upwards the other will be bent downwards and vice versa leading to thicker and thinner mantle transition zone, respectively.

The *d*410 and *d*660 are generally found to be sharp discontinuities (4–10 km thick) (Collier et al., 2001; Vidale et al., 1995; Yamazaki and Hirahara, 1994; Petersen et al., 1993; Benz and Vidale, 1993; Paulssen, 1988a). However, the sharpness of the phase transition intervals in the mantle transition zone can vary with temperature and water content. Decreased mantle temperatures lead to an increased *d*410 phase transition thickness and vice versa: a decrease in temperature of 800 K will broaden the phase transition interval with 10 km (Helffrich, 2000; Bina and Helffrich, 1994). The *d*660 phase transition interval, on the other hand, appears to remain sharp over a broad range of temperatures (e.g. Wood, 1990; Ito and Takahashi, 1989). The absence of short-period reflections from 520 km depth (Benz and Vidale, 1993; Jones et al., 1992; Cummins et al., 1992) compared to claims of global presence with long-period studies (Flanagan and Shearer, 1998; Shearer, 1990, 1991) could suggest that the *d*520 extends over a large depth interval of 25 up to 60 km (Akaogi et al., 1989) and possibly shows large topography.

Water has a larger influence on the sharpness of the discontinuities than temperature. In a hydrous mantle the *d*410 can broaden to as much as 40 km (Smyth and Frost, 2002; Helffrich and Wood, 1996; Wood, 1995). The *d*520 can be up to 60 km thick under anhydrous conditions (Akaogi et al., 1989) but an increased water content in the mantle transition zone can sharpen this phase transition interval to 15 km or less (Inoue et al., 1998). Excess water can also thicken the 660-km discontinuity, but its thickness would be at least five times less than that of the 410-km discontinuity for comparable amounts of water (Higo et al., 2001). However, because of increased seismogram noise levels at high frequencies such thickening is probably not observable with receiver functions analysis.

The Mediterranean mantle discontinuities have been only sparsely studied. Due to the global distribution of earthquakes and stations, it is not possible to obtain a good coverage for the Mediterranean region with *SS*-precursors that sample the mantle halfway between source and receiver. These studies result in only two local values for discontinuity depths in the Mediter-

ranean region (Gu and Dziewonski, 2002; Deuss and Woodhouse, 2001; Shearer, 2000). Source side conversions from *S*-to-*P* or *P*-to-*S* are not suitable for the Mediterranean region owing to a lack of deep events in this area with magnitude over 5.8. Receiver side *S*-to-*P* conversions are generally sensitive to noise and difficult to identify in complicated regions like the Mediterranean. The best method for detecting and analysing mantle discontinuities here is receiver side *P*-to-*S* conversions.

Receiver side studies that cover the Mediterranean region have not been performed yet. Chevrot et al. (1999) published results for a station in Spain and two stations in Turkey. Some preliminary results for Spain, Italy and Greece were presented by, e.g. Hanka et al. (2001) and Olivieri and Morelli (2001) while Li et al. (2003a) published results of a detailed study on the down going slab under southern Greece.

In this receiver function study we report on discontinuities in the upper- and lower mantle (between 300 and 1500 km depth) and estimate mantle transition zone thickness beneath 16 temporary and 6 permanent broadband seismic stations in the Mediterranean.

2. Data and method

2.1. Receiver functions

This study of mantle discontinuities in the Mediterranean region is facilitated by a recent, temporary deployment under the MIDSEA project of 25 mobile seismic broadband stations along the tectonic plate boundary between Eurasia and Africa (Van der Lee et al., 2001). We have analysed over 500 seismograms recorded in the Mediterranean region at 18 temporary broadband stations from this project and 6 permanent broadband stations (Fig. 1 and Table 1). Events are located between 30° and 95° epicentral distances, with most events coming from epicentral distances between 60° and 90° given the region's geographical location with respect to seismogenic zones. *P*-waves from these events partly convert to *S*-waves at mantle discontinuities beneath the stations. The converted phase is polarized as a *SV*-wave if the discontinuity is flat and is recorded on the radial component of the seismogram whereas the incoming *P*-wave is mainly recorded on the vertical component. Since the travel time of the con-

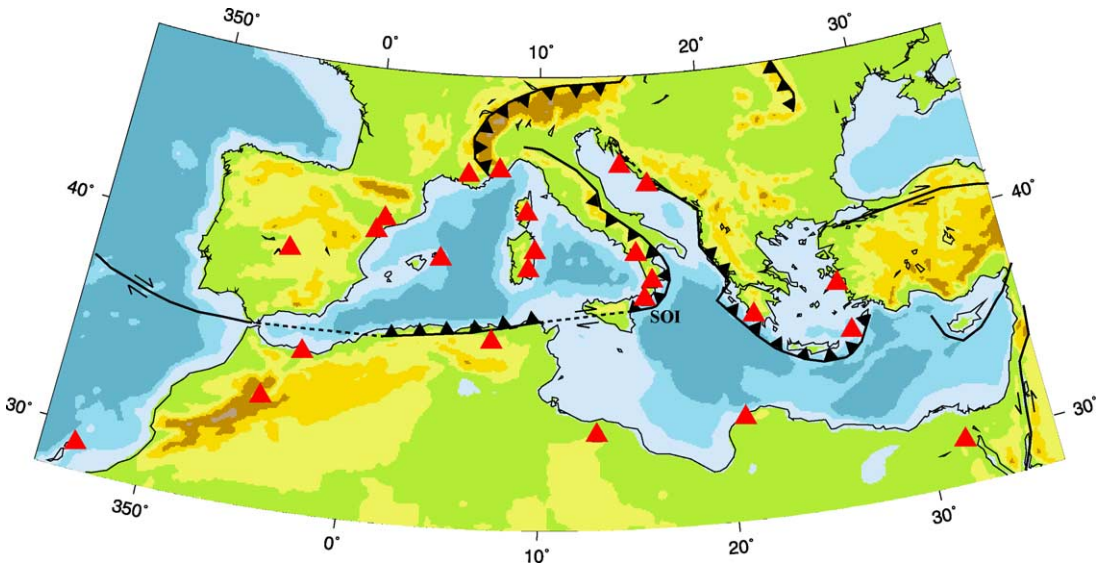

Fig. 1. Map of the Mediterranean region with seismic station and approximate plate boundary locations. Stations are represented by triangles and with the station name. Curves with sawtooth pattern indicate the present location of the convergent boundary, with sawtooth pointing in the direction of subduction or underthrusting. Strike-slip is represented by arrows. Blue colours indicate bathymetry (dark blue: deeper than 2.5 km; intermediate blue: 2.5–1.0 km; light blue: shallower than 1.0 km). Green-yellow colours represent topography (green: lower than 0.5 km; light yellow: 0.5–1.0 km; dark yellow: 1.0–1.5 km; brown: 1.5–2.5 km; grey: higher than 2.5 km).

Table 1
Locations of broadband stations, number of receiver functions used and resulting depth for different discontinuities in the upper mantle and thickness of the mantle transition zone

Station	Latitude	Longitude	*N*	*d*410	*d*520	*d*660	MTZ(km)
Europe							
PAB	39.546	−4.348	34	411	n.a.	668	257
POBL	41.380	1.080	12	*411*	485	*679*	*268*
EBRE	40.823	0.494	15	*386*	552	666	*280*
MAHO	39.896	4.267	8	435	571	708	273
VSL	39.496	9.378	29	415	n.a.	666	251
SMPL	42.094	9.285	16	395	*527*	640	245
DGI	40.318	9.607	15	418	*503*	662	244
RUSF	43.943	5.486	4	419	524	661	242
SAOF	43.986	7.553	16	413	489	674	261
MGR	40.138	15.553	17	393	501	670	277
GRI	38.822	16.420	10	396	475	678	282
SOI	38.073	16.055		Not robust			
DUOK	44.113	14.932	40	404	506	683	279
HVAR	43.178	16.449	23	418	507	664	246
ITHO	37.179	21.925		Not robust			
APER	35.550	27.174	34	414	517	661	247
KOUM	37.704	26.838	13	404	499	672	268
Africa							
CDLV	29.163	−13.444	9	*494*	*578*	713	*219*
MDT	32.817	−4.614	8	*400*	514	659	*259*
MELI	35.523	−2.939	11	409	*511*	*696*	*287*
ABSA	36.277	7.473	7	*410*	487	685	*275*
GHAR	32.122	13.089	8	413	*504*	634	221
MARJ	32.523	20.878	11	420	536	684	264
KEG	29.927	31.829	49	400	514	664	264

Depth estimates of converted phases and mantle transition zone thickness estimates that are not robust are printed in italic.

verted *SV*-wave is much smaller than that of the pure *S*-wave, we can conclude that every *SV*-wave arriving in the *P*-wave coda must have been converted from the *P*-wave. Therefore the identification of the *P*-to-*S* converted phases is less ambiguous than, for example, *S*-to-*P* conversions or *SS*-precursors.

Such converted waves can be identified with receiver function analysis (Ammon, 1991; Owens et al., 1984; Langston, 1979). A receiver function is constructed from each seismogram by deconvolving the vertical from the radial and transverse components. Before deconvolution the seismograms are high-pass filtered with a corner frequency of $f = 0.05$ Hz to remove possible long-period noise. In the deconvolution we apply time windows of 250 s, starting 20 s before the *P*-arrival, for the radial and transverse components of the seismogram. For the vertical component, which is representative for the incoming *P*-wave energy, we used a time window of 90 s, starting 20 s before the *P*-arrival, to obtain a more characteristic signal of the incoming *P*-wave. In the deconvolution process we applied a low-pass filter. For all stations we used a low-pass corner frequency of approximately $f = 0.25$ Hz or $f = 0.2$ Hz.

We compute the standard deviation of the stacked receiver function for the ith sample as $\sigma_i = \sqrt{\sum_{j=1}^{n}(r_{ij} - \overline{r_i})^2/(n(n-1))}$, where n is the number of receiver functions, r_{ij} the jth individual receiver functions, and $\overline{r_i}$ the stacked receiver function. We identify phases for which the mean stacked amplitude is larger than twice the corresponding standard deviation and therefore non-zero with 95% confidence. To test the information content of receiver function stacks based on only seven or more receiver functions we applied a bootstrapping technique to the receiver functions of PAB and DUOK. We randomly selected 20% of the total number of receiver functions for each station and calculated the stack for this subset. The re-

sulting stacks generally fall within the 95% confidence interval for the full stack of receiver functions.

2.2. Depth conversion

For each receiver function we used a local reference seismic-velocity model (Li et al., 2002; Dueker and Sheehan, 1998) to compute expected arrival times of *P*-to-*S* converted phases for conversion depths every 200 m. We evaluated the receiver function value at the predicted time and assigned it to the corresponding depth. This procedure corrects for move-out curves of any shape (Gurrola et al., 1994). The move-out and time to depth converted receiver functions were stacked over all events analysed for each station. The advantage of stacking in the depth domain is that discontinuity related phases will stack more coherently compared to stacking along constant-slowness lines in the time domain. This difference is discussed more specifically for a site in Spain in Section 3.1.

The local seismic-velocity models used to convert the receiver functions' time axes to depth are extracted from the three-dimensional *S*-velocity model for the Mediterranean region of Marone et al. (2004) (hereinafter referred to as EAV03). Using crystal thickness estimates from Van der Meijde et al. (2003a) and Marone et al. (2003), specifically for the analysed stations, and upper mantle and transition zone velocity models from Marone et al. (2004) we have corrected the receiver functions for laterally varying velocity structures in the Mediterranean region. *P*-wave velocities (Vp) were obtained by scaling each local *S*-velocity (Vs) model with Vp/Vs ratios from IASP91 (Kennett and Engdahl, 1991).

2.3. Error analysis

The EAV03 model, which we use for the time-to-depth conversion of our receiver functions, is a non-unique explanation of regional seismograms and may therefore deviate from the actual local *S*-velocity. Furthermore, we estimate the *P*-velocity using the Poisson ratio from IASP91 (Kennett and Engdahl, 1991). This estimate may be incorrect for conditions that decrease seismic velocities, such as high mantle temperature, occurrence of melt and/or fluids or chemical composition that have a significantly larger effect on *S*- rather than on *P*-velocities (Cammarano et al., 2003). For example, a low velocity zone could be stronger for *S*-velocities than for *P*-velocities, which results in a relatively high Poisson ratio. Errors in the estimated *P*- and *S*-velocities can cause significant errors in estimates of the absolute depth of mantle discontinuities and transition zone thickness.

Assuming correlated Vp and Vs, with wave velocity uncertainties of ±1%, the maximum uncertainty in discontinuity depth is 4 km for the *d*410 and 6 km for the *d*660. If Vp and Vs are uncorrelated, i.e. no fixed Poisson ratio, the uncertainties are as large as 10 km for the *d*410 and 14 km for the *d*660. Uncertainties in picking the exact depth of the maximum amplitude of the converted phase and dependence of the picked depth on frequency content of the receiver functions (Van der Meijde et al., 2003b) result in estimated errors of 6 km for the *d*410 and 3 km for the *d*660. The conversion model does not include discontinuity up- or down warp which results in a variation in the estimated discontinuity depth of 1 km for both *d*410 and *d*660 for every 20 km elevation.

If we assume a maximum deviation of the reference *S*-velocity model of 0.5% with an additional 0.5% uncertainty in the *P*-velocities (approximately 0.1 km/s) we can estimate the total error on the obtained absolute depth estimate from all aforementioned error components. The uncertainties in the reference wave speed model contributes 7 km for the *d*410 and 10 km for the *d*660. Uncertainties in the picking and unmodeled discontinuity elevation account for an additional 7 km for *d*410 and 4 km for the *d*660. The total error budget for the absolute depth estimate of the discontinuities is 14 km for both *d*410 and *d*660. The thickness estimate of the mantle transition zone (*d*660–*d*410) has an error of ±9 km. This is the sum of 3 km due to the velocity model and 6 km owing to the picking of the converted phases.

3. Results

We carried out a systematic search for converted phases beneath 24 stations in both the northern and southern Mediterranean region (Fig. 2). We took into account only converted phases that are significant at the 95% confidence level, i.e. amplitudes that are non-zero within the double standard deviation of the stack of single receiver functions. Although locally results can

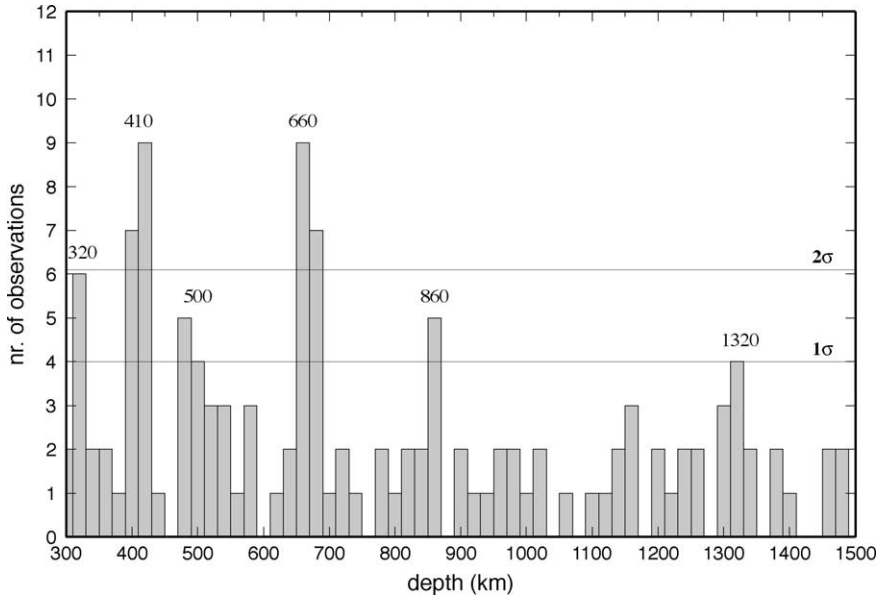

Fig. 2. Histogram with the number of counts of significant converted phases observed in 22 stacked receiver functions. The bin size is 20 km. Only used the significant converted phases account for this figure. However, using all converted phases (significant or not) results in a similar figure. Numbers are higher but the shape and locations of the peaks are essentially the same.

vary with the choice of the bin size in depth (15, 20, or 25 km bin size), we observe (Fig. 2), with 95% confidence (2σ), converted phases from 410 km and 660 km depth. Additional converted phases, within 67% confidence (1σ), are observed around 320 km, 500 km, 850 km and 1320 km depth.

In the following, we present estimates for mantle transition zone discontinuity depth and thickness in the northern and southern Mediterranean region. In Figs. 3 and 4 and Table 1 we summarize the results of the receiver function analysis for mantle transition zone thickness underneath 24 stations in the northern and southern Mediterranean region, respectively. We adopt reference depths for the discontinuities from the reference seismic-velocity model (Marone et al., 2004). These are 410 km for the *d*410, 520 km for the *d*520, 660 km for the *d*660 and 250 km for the thickness of the mantle transition zone.

All conversions from anomalous transition zone thickness to temperature are based on Clapeyron slopes for the *d*410 and *d*660 of 3.1 MPa K^{-1} (Helffrich, 2000) and -2.0 MPa K^{-1} (Bina and Helffrich, 1994), respectively. The transition zone thickness in our reference model represents a thermal regime about 90 K colder than the global average (Flanagan and Shearer, 1998).

In the next chapter we will discuss in more detail the anomalous amplitudes of the converted phases from the *d*410 and *d*660, strong conversions observed from the *d*520, possible upper- and lower mantle discontinuities and relate the mantle transition zone thickness with tectonic processes in the Mediterranean.

3.1. Transition zone structure in the northern Mediterranean

Underneath station PAB in central Spain, the *d*410 and *d*660 are observed at 411 ± 14 km and 668 ± 14 km depth, respectively, resulting in an undisturbed mantle transition zone thickness of 257 ± 9 km. With data stacked for PAB having western or northern backazimuths, a high velocity body between 300 and 550 km under eastern Spain (Marone et al., 2004) has not been sampled by these data. Previous studies did not find significant converted energy from the *d*410 beneath this station (Chevrot et al., 1999; Hanka et al., 2001; Olivieri and Morelli, 2001). The first of two possible explanations for the missing *d*410 in previous studies could be that receiver functions were low-passed filtered with corner frequencies over 2 s (Van der Meijde et al., 2003b). The second is that

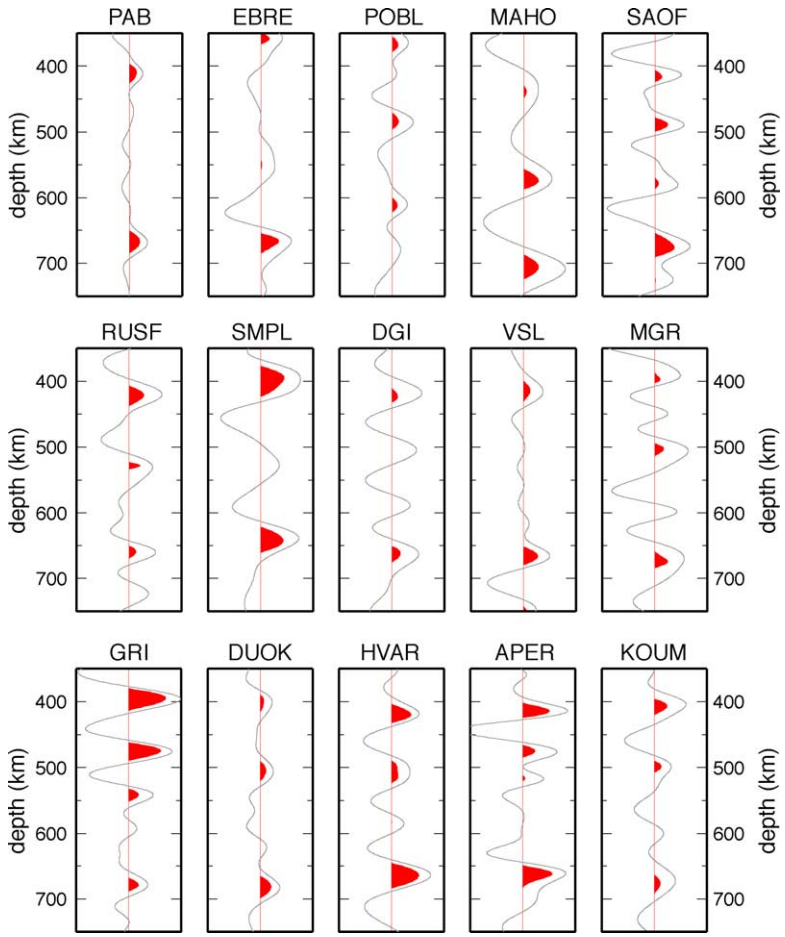

Fig. 3. Receiver functions for the stations on the Eurasian plate in the depth range between 350 and 750 km depth. Time is converted to depth using local models extracted from EAV03 (Marone et al., 2004). Red colors indicate phases for which the mean stacked amplitude is larger than twice the corresponding standard deviation and therefore non-zero with 95%.

stacking along a constant-slowness line (Chevrot et al., 1999) does not stack *P*410*s* as coherently as with our corrections for curved move-out. We tested stacking along a constant-slowness line, rather than stacking in the depth domain, on our data set. In the receiver function obtained from the constant-slowness stack we did not observe a significant conversion from the *d*410.

For EBRE and POBL we observe significant conversions from some but not all transition zone discontinuities. We observe relatively weak *P*-to-*S* converted energy from the *d*410 under eastern Spain. This could indicate that the *d*410 here is not sharp. The *d*410 cold have been thickened by lower temperatures (Helffrich and Bina, 1994) and/or raised water contents (Wood, 1995). A high seismic-velocity body imaged at this depth beneath this region (Marone et al., 2004) could account for both conditions if it represents oceanic lithosphere that subducted during the palaeocene (Marone et al., 2004). Such oceanic lithosphere would still be relatively cold and have brought water down to transition zone depths. Nearby station PAB has been found to possibly overlie a 30–35 km thick *d*410, which is inferred to have thickened by near 1000 wt. ppm of water in sup-*d*410 olivine (Van der Meijde et al., 2003b). Similar conditions could exist beneath EBRE and POBL. Such cold and wet conditions, combined with fewer seismograms and lower signal to noise ratios compared to station PAB, could explain the

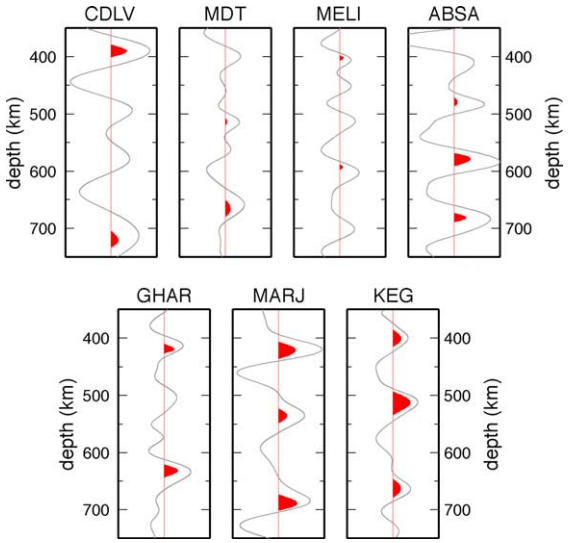

Fig. 4. Receiver functions for stations on the African plate in the depth range between 350 and 750 km depth. Time is converted to depth using local models extracted from EAV03 (Marone et al., 2004). Red colors indicate phases for which the mean stacked amplitude is larger than twice the corresponding standard deviation and therefore non-zero with 95%.

observed weak *P*410*s* energy. We suspect that topography on the *d*660, related to the same cold, high-velocity body, might be responsible for incoherent stacking of *P*410*s* for POBL, which is located near the edge of the high-velocity body (Lebedev et al., 2002; Van der Lee et al., 1994). However, the stark differences between the receiver functions of these two stations in north-eastern Spain present a good case for a focused investigation with several broadband stations deployed there for more than two years.

More to the east the high velocity anomaly extends till deeper depths under MAHO (Marone et al., 2004). This is consistent with our observation of an increased thickness of the transition zone of 23 km (273 ± 9 km). We observe a shift of all transition zone discontinuities to greater depths with ∼25 km. This shift indicates that we may have underestimated the velocities in the local velocity model for the island by adopting the low velocities modeled for the entire region: The Algero-Provençal Basin. Local deviations of regional velocity structure are not accounted for in the error analysis and can be the cause of additional uncertainties in the depth conversion of the receiver functions. A 4–5% local velocity adjustment in the upper 400 km would be needed to shift the *P*410*s* back to 410 km. The resulting velocity model is then similar to *iasp91*. The teleseismic delay time measurements of Schmid et al. (2004) at station MAHO supports the notion of a relatively normal vertical velocity average beneath Menorca by showing the delays to be close to the Mediterranean average.

Despite the low number of receiver functions for RUSF, we report a relatively normal transition zone thickness under this station of 242 ± 9 km (Fig. 3) because each of the 4 individual receiver functions is unusually coherent with the other 3. We observe a thick transition zone (261 ± 9 km) for SAOF. Tomographic *P*-velocity models (Wortel and Spakman, 2000; Morelli and Piromallo, 2000) show a high velocity anomaly in the mantle transition zone under the Ligurian Sea, just east of SAOF, which is also present in EAV03 at the bottom of the transition zone, though with a smaller amplitude. This could explain the observed broadening of 11 km, which relates to decreased temperatures at the bottom of the mantle transition zone by 180 K.

The thickness of the mantle transition zone under Corsica and Sardinia (SMPL, DGI and VSL) is relatively normal (between 244 ± 9 km and 251 ± 9 km). Especially the receiver functions for nearby stations VSL and DGI look similar, both in shape and in absolute depth of the *d*410 and *d*660 which are observed around 415 ± 14 km and 665 ± 14 km depth, respectively (Fig. 3). The *d*410 and *d*660 below SMPL are at 395 ± 14 km and 640 ± 14 km, respectively. This uplift of the discontinuities under SMPL could be an artefact caused by a −9% low velocity anomaly, relative to *iasp91*, in the upper most mantle of EAV03, that is less pronounced in *P*-velocity models (Wortel and Spakman, 2000; Morelli and Piromallo, 2000). Because we assumed a constant Poisson ratio we could have underestimate the *P*-velocities in our time-to-depth conversion and thereby underestimate the depths of the discontinuities: Two percent faster *P*-velocities than used in our local model (which are still slower than predicted by IASP91) will increase our depth estimates for the discontinuities by 18 km, resulting in similar depths for the transition zone discontinuities as observed for DGI and VSL. The relatively undisturbed mantle transition zone is not supported by tomographic *P*-velocity models that show a high-velocity anomaly around 600–700 km depth. If *P*-velocities in our local velocity model are underestimated with 2%, which

is possible since the anomaly is less pronounced in EAV03 than in the *P*-velocity models, the transition zone could be maximum 10 km thicker.

Under southern Italy we observe a thick transition zone under MGR, GRI (Fig. 3). The thickness increases towards the south. The northern station MGR has a 277 ± 9 km thick transition zone whereas under the southern station GRI the thickness increases up to 282 ± 9 km. Both discontinuities contribute to the thick mantle transition zone. We observe significant uplift of the *d*410 under both stations of ∼15 km while under GRI we also observe a significant 18 km down warp of the *d*660 whereas the down warp under MGR is 10 km. This is in agreement with the steeply dipping slab east of the stations (Faccenna et al., 2003), which reaches the transition zone in the vicinity of the conversion points beneath these stations. The broadened mantle transition zone under southern Italy could be related to a maximum temperature anomaly of 300 K, possibly related to the down going slab. This is much smaller than temperature anomalies of up to 600 K observed in steeply dipping slabs in Asia by, e.g. Collier and Helffrich (1997). For SOI most stacks do indicate a thick mantle transition zone but no stable stacks were obtained due to a high background noise level. Therefore it was not possible to constrain transition zone thickness under this station.

Stations DUOK and HVAR in Croatia recorded uninterrupted in low-noise environments (Van der Lee et al., 2001). This resulted in the recording of a large number of suitable events and a high signal to noise ratio for the stacked receiver functions showing significant conversions for the *d*410, *d*520 and *d*660 for both stations. The northernmost station DUOK shows a mantle transition zone that is thickened by more than 25 ± 9 km. This is the result of a combined effect from an upwarp of the *d*410 and a downwarp of the *d*660. The station HVAR, more to the south, has an average transition zone thickness. No significant variations in the depth of the discontinuities is observed here. The difference in transition zone thickness between these two sites may reflect a laterally varying tectonic history that might have cooled the transition zone more in the northern Adriatic region than in the central Adriatic region. Again, this relatively well constrained difference warrants a focused investigation deploying several broadband stations for more than 2 years along and across the Adriatic Sea and Dinarides.

Close to the Hellenic trench we observe a transition zone of average thickness (247 ± 9 km) underneath station APER with clear conversions from both 410- and 660-discontinuity at 414 ± 14 km and 661 ± 14 km depth, respectively (Fig. 3). Further north we observe a thick mantle transition zone of 268 ± 9 km underneath KOUM. *d*410 and *d*660 are uplifted by 6 km and down warped by 12 km, respectively. We estimate the temperature drop to be between 70 and 200 K. This is in good agreement with the presence of a high velocity anomaly in the transition zone in *P*- and *S*-velocity models related to the subduction of African lithosphere at the Hellenic trench (Marone et al., 2004; Wortel and Spakman, 2000; Morelli and Piromallo, 2000), and with a receiver function study by Li et al. (2001) showing conversions from the down going slab at transition zone depth in the vicinity of this station. The down going slab probably prevents us from obtaining significant converted energy from transition zone discontinuities for ITHO. We observe a strong signal around 200–220 km depth, most likely related to the down going slab. The slab probably scatters the energy of the *P*-to-*S* converted phases from transition zone discontinuities resulting in unstable stacks with not enough *P*-to-*S* converted energy on the radial component to resolve the mantle transition zone thickness underneath this station.

3.2. Transition zone thickness in the southern Mediterranean

The stations in northern Africa are located at the edge of the considered Mediterranean velocity model EAV03 that we use to estimate the discontinuity depths. At this edge, the resolution is reduced, especially at transition zone depths yielding our time-to-depth conversion less reliable than for stations in the northern Mediterranean. Mantle transition zone thickness and discontinuity depths thus have larger uncertainties here of 18 km for the absolute depth estimate for the *d*410, 20 km for the *d*660 and 11 km for the thickness estimate of the transition zone (corresponding to an additional ±1% uncertainty in EAV03 compared to the northern Mediterranean). On average, we observe relatively thick transition zone (260–275 km) in northern Africa (Fig. 4).

For both MARJ and KEG the observed mantle transition zone thickness is 264 ± 11 km, 14 km more than

the reference thickness (Fig. 4). The thickened transition zone under KEG and MARJ is consistent with a high velocity anomaly at the bottom of the mantle transition zone under northern Egypt and north-eastern Libya observed in EAV03 (Marone et al., 2004). GHAR's receiver functions show clear conversions from both *d*410 and *d*660 (Fig. 4). The *d*410 is relatively undisturbed and observed around 413 ± 18 km depth while the *d*660 shows an upwarp of more than 25 km resulting in a thin mantle transition zone of 221 ± 11 km. This upwarp implies an unlikely temperature deviation of over 400 K. Unless such a high temperature, and the low velocities in EAV03 that were used to estimate this shallow depth for the *d*660, are related to the Mount Etna or an unknown mantle plume (Marone et al., 2004; Montelli et al., 1999), we consider the upwarp to be unlikely. In the latter interpretation our receiver functions would invalidate low velocities imaged below GHAR in EAV03, which is perfectly acceptable given the low resolution and associated "smearing" for EAV03 this deep at the edge of the model.

For ABSA, MELI and MDT we observe significant conversions from some but not all transition zone discontinuities (Fig. 4). Beneath MELI, the *d*410 is observed at 409 ± 18 km. Conversions from the bottom of the mantle transition zone are significant only for ABSA and MDT. For the *d*660 we do observe a clear conversion for ABSA at 685 ± 20 km resulting in a transition zone thickness estimate of 275 ± 11 km. We do not observe a robust signal from the *d*660 underneath MELI. The thick transition zone observed beneath north-western Africa is likely related to remnants of a subducted slab under northern Morocco and Algeria, visible as a high-velocity anomaly in EAV03 (Marone et al., 2004).

For station CDLV on the Canary island Lanzarote only nine receiver functions had sufficient signal to noise ratios for stacking. Furthermore, the absolute depth and corresponding uncertainties of the discontinuities beneath the island Lanzarote, part of the Canary Islands, are not resolved because the local model is not well resolved beneath 200 km. However, using the *iasp91* reference velocity model yields shallower discontinuity depths and a peak not significant at the 95% confidence level near 410 km. The thus estimated transition zone thickness is 219 ± 11 km, which is 31 km thinner (and 200 K warmer) than the reference mantle transition zone thickness and 23 km thinner than the globally averaged transition zone thickness. However, this thickness contrasts with recent findings that the transition zone is only about 10 km thinner beneath the few hundreds of km removed, former GSN station TBT (Li et al., 2003b). To reduce the large uncertainty for the transition zone beneath Lanzarote more broadband stations need to operate for more than 3 years in this high-noise environment of the Canary Islands to obtain a more robust estimate of transition zone thickness.

4. Discussion

Simple, unweighted averaging of the spatially unevenly distributed estimates of transition zone thickness in the Mediterranean mantle yields a thickness of 261 ± 9 km. This average thickness of the Mediterranean mantle transition zone is 19 km larger than the global average of 242 km deduced from *SS*-precursor studies (Flanagan and Shearer, 1998). An increased transition zone thickness of 19 km relates to temperatures reduced by 120 K between 410 and 660 km depth. Using the results of Cammarano et al. (2003) we can infer the velocity difference due to this temperature effect to be 1% in Vs and 0.6% in Vp relative to *iasp91*. These estimates agree with high average velocities in the transition zone imaged in tomographic models (Marone et al., 2004; Wortel and Spakman, 2000; Morelli and Piromallo, 2000). We verified that this agreement cannot be explained by mis-estimated transition zone velocities in our time-to-depth conversions. We observe a correlation between the location of the plate boundary, high velocity anomalies imaged in tomographic models and thick transition zone estimates (Fig. 5). We found strongly thickened transition zone (>270 km) related to past subduction underneath eastern Spain, southern Italy and the north-western African coast. Thinned transition zone is only observed beneath two stations, CDLV and GHAR. The reference velocity models are not well constrained for these stations, especially below 400 km and therefore mantle transition zone thickness estimates remain uncertain.

4.1. Velocity contrasts

From the amplitudes of the converted phases we can estimate the impedance contrast at the discontinuities. The Mediterranean-wide average amplitude of *P*-to-*S*

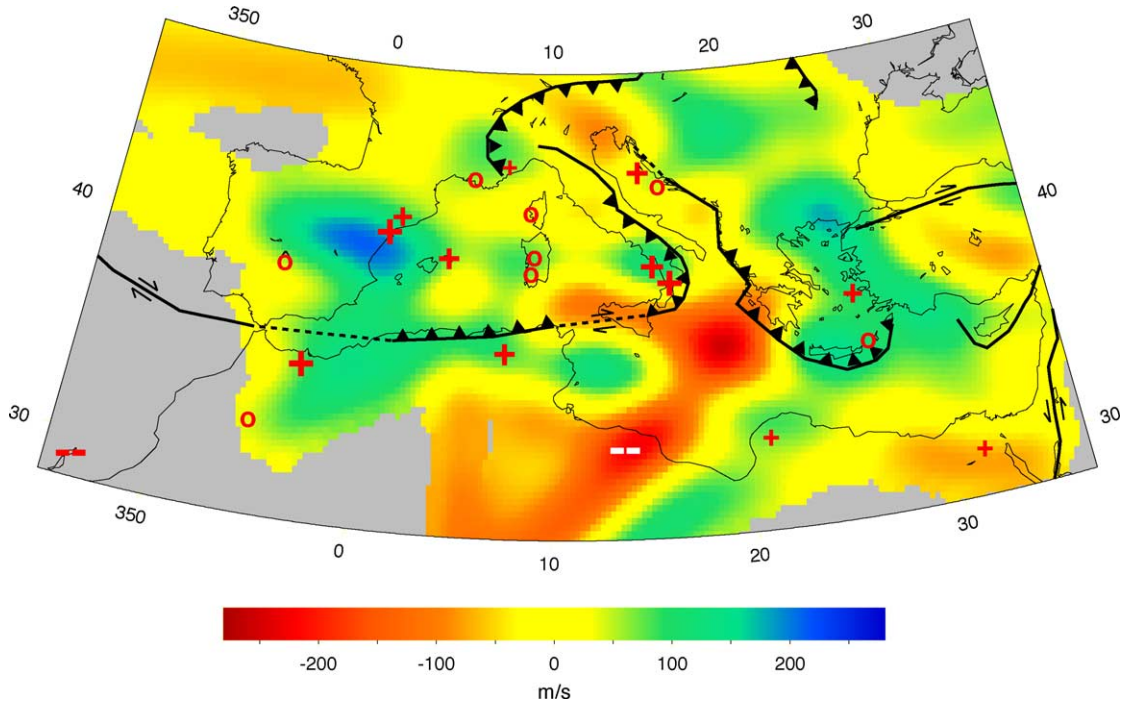

Fig. 5. Results for mantle transition zone thickness. A zero means no significant thicker or thinner transition zone (250 ± 10 km), a thick transition zone is indicated by a plus, scaled for thickness. Similar for a thin transition zone. The tomographic model is the mean velocity in the transition zone from EAV03 (Marone et al., 2004). A clear correlation is visible between transition zone thickness, velocity anomalies and location of the plate boundary.

converted phases is based on the amplitudes of these phases in the stacks for each station, whether or not it showed the converted with more than 95% confidence, taking into account the corresponding standard deviations. In the Mediterranean region, the mean $P_{410}s$ amplitude is $0.049 \pm 0.028(2\sigma)$ and the $P_{660}s$ amplitude is $0.057 \pm 0.024(2\sigma)$, relative to a unit amplitude *P*-arrival. We used all stations for this calculation, including the ones without significant conversions for that specific discontinuity. Both values are larger than predicted by global models for 82.5 degrees epicentral distance (the average epicentral distance in our data set) (Kennett et al., 1995; Morelli and Dziewonski, 1993; Kennett and Engdahl, 1991; Dziewonski and Anderson, 1981). However, the global values for $P_{410}s$ and $P_{660}s$ lie within 2σ of our observed values. They predict an average amplitude of 0.021 for the $P_{410}s$, and 0.041 for the $P_{660}s$. Such anomalous amplitudes have previously been observed by Helffrich et al. (2003) and Shearer and Flanagan (1999). In the Mediterranean region we found an anomalously thick *d*410 (Van der Meijde et al., 2003b). A thick discontinuity can reduce the amplitudes of the converted phases. In our interpretation we use low frequency receiver functions, so estimates for the velocity contrast at the *d*410 are as accurate as possible. Synthetic modelling (Van der Meijde et al., 2003b) shows that topography on the discontinuity causes different amplitude effects than what we observed for the *d*410.

From a receiver function study, Helffrich et al. (2003) found an anomalous $P_{410}s$ amplitude under the northern UK, which is twice as large as predicted by the global models and close to our value. Their anomalous $P_{660}s$ amplitude is much smaller than our and global observations with $0.029 \pm 0.017(2\sigma)$.

In a global study of amplitudes of *SS*- and *PP*-precursors Shearer and Flanagan (1999) suggest that global models overestimate the amplitudes for reflections of the *d*660 and underestimate those of the *d*410. This agrees with the high $P_{410}s$ amplitude we found

throughout the Mediterranean region. Their estimate for the velocity contrast at the *d*410 is twice as large as predicted by global models. Such a contrast results in a $P_{410}s$ amplitude of 0.050, which is remarkably close to our observed value of 0.049.

Our slightly high value for $P_{660}s$ could arise from decreased attenuation in the transition zone underneath the Mediterranean region. This is supported by the presence of high velocities in the lower half of the upper mantle (Marone et al., 2004; Piromallo and Morelli, 2003; Wortel and Spakman, 2000) which can decrease the attenuation (Aki and Richards, 2002), resulting in higher amplitudes. High velocity anomalies, related to anomalous transition zone composition, can thus be responsible for the observed $P_{660}s$ amplitude.

4.2. Mid-transition zone discontinuity around 520 km depth

There are different hypotheses about the nature of the *d*520 but in general it is thought that the transition from wadsleyite to ringwoodite is responsible for this discontinuity (Katsura and Ito, 1989). This phase change has a large positive Clapeyron slope (5.1 MPa K^{-1}). Estimates for the impedance contrast vary strongly from less than 1% (Cummins et al., 1992; Jones et al., 1992), via 2–3% (Gu et al., 1998; Gossler and Kind, 1996; Shearer, 1990) up to 5–6% (Inoue et al., 1998; Rigden et al., 1991). The phase transition interval is relatively wide under anhydrous conditions, estimates are as high as 60 km (Akaogi et al., 1989). However, a recent study shows that the presence of water can sharpen the *d*520 to 15 km or less (Inoue et al., 1998). We found strong energy from phases converted at a discontinuity between 450–550 km depth for most stations in the Mediterranean region (Figs. 2–4), which we relate to the aforementioned *d*520. Large variances in depth for the *d*520 are observed in Fig. 2. The *d*520 does not appear as consistently at the same depths as the *d*410 and the *d*660; its depth possibly spans 60–80 km, which is at least 20–40 km more than the *d*410 and *d*660. This seems to be a global characteristic, as Chevrot et al. (1999) found a variation in depth of the *d*520 of approximately 50 km worldwide.

Although we do not observe significant conversions for all stations, it appears that the *d*520 has a relatively strong impedance contrast as $P_{520}s \sim 0.036 \pm 0.032(2\sigma)$, and occurs over a phase transition interval throughout most of the Mediterranean region that is relatively thin in places. The frequency content of the receiver function stacks suggests that the *d*520 could be at least as thin as 20 km below those stations showing a significant *P*520*s*. Temperature plays a role in the sharpness of the *d*520. The transition from wadsleyite to ringwoodite becomes much thinner for relatively high temperatures (Helffrich and Bina, 1994; Bina and Wood, 1987). However, in the Mediterranean region we do not find a clear correlation between the coexistence of a sharp *d*520 and a warmer transition zone. In general, the Mediterranean mantle transition zone is found to have relatively fast velocities compared to global models (Marone et al., 2004; Wortel and Spakman, 2000; Morelli and Piromallo, 2000) resulting in low temperatures (Cammarano et al., 2003). This would actually suggest that the *d*520 is broad and less visible in receiver functions. Because this is inconsistent with our observations, we conclude that temperature differences are not the main influence on the thickness of the 520-km phase transition interval. A significant amount of water may be present in the Mediterranean mantle as shown by Van der Meijde et al. (2003b). They found that up to 700–1000 ppm of water can be present around 400 km depth in olivine, and possibly extending deeper into the mantle transition zone. Such an amount of water would lead to a thinned *d*520 (Inoue et al., 1998), which is consistent with our observations. However, there is no positive correlation between the estimated thickening of the *d*410 and a thinning of the *d*520 (Van der Meijde et al., 2003b), suggesting that water may not be homogeneously distributed in the transition zone.

For some stations we observe double conversions in the depth range between 450 and 550 km (e.g. GRI, APER, SAOF). In high frequency receiver functions this split is also visible for the stations in Croatia (HVAR and DUOK) (Van der Meijde et al., 2003b). High frequencies ($f = 0.35$–0.8 Hz) show a double peak that becomes less sharp below 0.3 Hz and finally indistinguishable below 0.2 Hz, forming one broad peak. Recently, Deuss and Woodhouse (2001) presented evidence of such splitting of the *d*520 from *SS*-precursors. However, their data point in the eastern Mediterranean did not show a split *d*520. However, we also observe a single, unsplit *d*520 in the frequency range they used (15–75 s).

Several explanations are possible for a split transition around 520 km depth. The main phase transition at

this depth is the transition from wadsleyite to ringwoodite. Another variant of wadsleyite is reported by Smyth and Kawamoto (1997) who suggest a wadsleyite-II phase, which is intermediate in density and pressure stability between wadsleyite and ringwoodite. It may require a significant amount of water and Al for stabilization. Since a significant amount of water could be present in the Mediterranean mantle transition zone (Van der Meijde et al., 2003b) this phase could be stable and responsible for a split *d*520. Deuss and Woodhouse (2001) explained the split of the *d*520 by the double transition from diopside via Ca-rich perovskite, Mg-rich spinel and stishovite to Ca-rich perovskite and ilmenite which takes place at this depth within 1 GPa (less than 30 km) (Koito et al., 1996; Ita and Stixrude, 1992). Depending on water content, temperature and chemical composition of the mantle transition zone, a single, or double transition can be observed.

4.3. 320 km discontinuity

In Fig. 2 a possible discontinuity in the upper mantle is observed around 320 km depth. A discontinuity around 320 km depth has been previously observed (Li et al., 2002; Deuss and Woodhouse, 2002; Gu et al., 1998; Leven, 1985), though differently interpreted. Li et al. (2002) related the discontinuous structure to a change in rheological properties in the low velocity

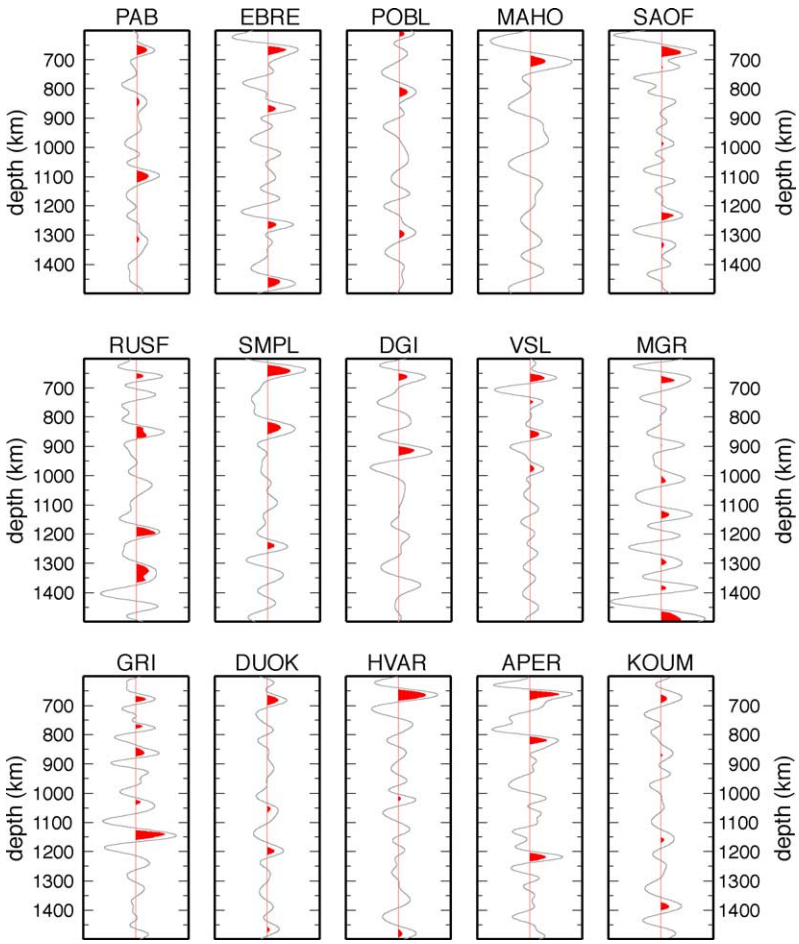

Fig. 6. Receiver functions for the stations on the Eurasian plate in the depth range between 600 and 1500 km depth. Time is converted to depth using local models extracted from EAV03 (Marone et al., 2004). Red colors indicate phases for which the mean stacked amplitude is larger than twice the corresponding standard deviation and therefore non-zero with 95%.

zone underlying the north-American keel. A chemical explanation is given by Deuss and Woodhouse (2002): the discontinuity may be caused by a phase change in Ca-poor pyroxene. In a Ca-poor mantle composition this phase transition interval occurs around 300 km depth and can be as thin as 5–6 km (Woodland, 1998). However, a depleted mantle is not likely to be present in the Mediterranean region because of the presence of water around 400 km depth (Van der Meijde et al., 2003b) which suggests a undepleted mantle (Karato, 2003). Small variations in Ca content will broaden the phase transition interval, possibly up to 30 km (Woodland, 1998), and make it less observable with receiver function studies.

4.4. Lower mantle discontinuities

Reports on lower mantle discontinuities are often based on studies of regions with active subduction (e.g. Kawakatsu and Niu, 1994). In many cases they are limited to the upper 400 km of the lower mantle, where relatively high gradients in velocity and density can occur (Karato and Ohtani, 1992). However, a few were observed outside subduction zones (Le Stunff et al., 1995; Paulssen, 1988b). Fig. 2 shows the total count of significant converted phases per depth interval that gives an overview of the significant phases visible in our receiver functions. We observe significant ($\sim 1\sigma$) converted energy from discontinuities around 860 and 1320 km depth. Figs. 6 and 7 shows the corresponding receiver functions between 600 and 1500 km depth.

The conversion at 850 km depth could be related to a change in crystal symmetry of perovskite that is thought to happen around this depth (Wang et al., 1992). Also Paulssen (1988b) and Le Stunff et al. (1995) did find indications for a discontinuity around 800–860 km depth under western Europe and southern Africa.

Significant conversions are observed for depths around 1325 km. Previous observations of discontinuous structure around this depth are made by Deuss and Woodhouse (2002) and Castle and Van der Hilst (2003), however, there is no obvious phase change described in the literature at this depth.

Figs. 6 and 7 show prominent converted phases at other depths but their number does make these significant at less than (1σ) (Fig. 2). This could be a result of strong lateral variations in depth and/or thickness. More data would allow the observed conversions

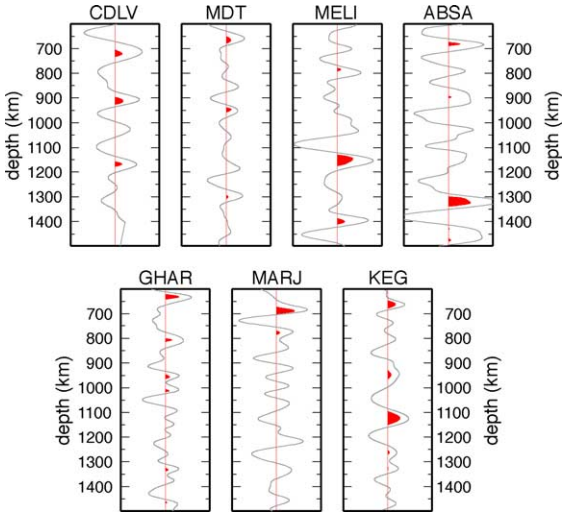

Fig. 7. Receiver functions for stations on the African plate in the depth range between 600 and 1500 km depth. Time is converted to depth using local models extracted from EAV03 (Marone et al., 2004). Red colors indicate phases for which the mean stacked amplitude is larger than twice the corresponding standard deviation and therefore non-zero with 95%.

to become more significant if they were generated by a laterally coherent and relatively sharp discontinuity. We observe (Figs. 6 and 7) that 18 stations show converted energy from clusters around 920–960 km, 1020–1040 km, 1180–1220 km and 1460–1480 km depth. The conversions around 920–960 km depth are clearly separated from the conversion around 860 km depth. Other evidence for a discontinuity around 920 km depth is presented by Kawakatsu and Niu (1994). In a later paper Niu and Kawakatsu (1997) showed that this discontinuity varies in depth between 900–1080 km. Additional evidence for lower mantle discontinuities is presented by Vinnik et al. (2001), who propose discontinuities at 900 and 1200 km depth. Under southern Africa a discontinuity was found around 1200 km depth by Le Stunff et al. (1995).

5. Conclusion

Receiver function analysis of *P*-to-*S* converted phases under the Mediterranean region reveals several seismic discontinuities in the upper- and lower mantle. *S* phases converted from *P* at discontinuities bordering the mantle transition zone, *d*410 and *d*660, are clearly

observed for the majority of the analysed stations. We use these observations to estimate the depth of these discontinuities and, with higher accuracy, the thickness of the mantle transition zone. Under the Mediterranean region we observe, on average, a thick mantle transition zone of 261 ± 9 km. This increased thickness is consistent with lower temperatures expected from high velocities in the mantle transition zone in tomographic models. In regions affected by ongoing or past subduction (eastern Spain, southern Italy, southern Greece and the north-western African coast) thickening of the mantle transition zone with 10–30 km is observed (Table 1). We estimate the maximum temperature anomaly related to these thick transition zones and associated subduction to be near 300 K.

The mean $P_{410}s$ amplitude in the Mediterranean region is $0.049 \pm 0.028(2\sigma)$, which is in agreement with previous studies in other regions (Helffrich et al., 2003; Shearer and Flanagan, 1999) but twice as large as expected from global models (Kennett et al., 1995; Morelli and Dziewonski, 1993; Kennett and Engdahl, 1991; Dziewonski and Anderson, 1981). The $P_{660}s$ amplitude is with $0.057 \pm 0.024(2\sigma)$ 10–60% larger as proposed in previous studies or expected from global models. We have observed significant conversions from the 520 km discontinuity. This phase transition interval is normally relatively thick, and therefore not usually observed in receiver function studies. For the Mediterranean region we suggest that the transition interval is relatively narrow, locally occurs over less than 20 km, and has a relatively strong impedance contrast ($P_{520}s \sim 0.036 \pm 0.032(2\sigma)$). Increased water contents in the mantle transition zone as evidenced by a thickened 410-km discontinuity (Van der Meijde et al., 2003b) could also be responsible for the increased visibility of $P520s$ (Inoue et al., 1998). The absolute depth of the $d520$ is variable: converted phases are observed over a depth interval of over 60–80 km. We found a split of the discontinuity beneath the Adriatic Sea, Greece and Italy.

An upper mantle discontinuity is found around depths of 320 km beneath some stations. In a Ca-poor mantle composition a phase change in Ca-poor pyroxene could be responsible for this discontinuity (Woodland, 1998). The thickness of this phase transition interval can, theoretically, vary between 5 km and 30 km, depending on the Al and Ca contents of pyroxene, which is probably the reason why we do not observe it for all stations.

The Mediterranean lower mantle structure also produces spatially incoherent *P*-to-*S* conversions from apparent depths between 700 and 1500 km. Converted phases from around 860 km are possibly related to a discontinuous change in crystal symmetry of perovskite (Wang et al., 1992).

Acknowledgements

Funding for this study was provided by the Swiss National Science Foundation (SNF). Financial support for MIDSEA came from the SNF, with additional support from the Carnegie Institution of Washington, the French National Scientific Research Center and the University of Nice at Sophia-Antipolis, the Italian National Institute of Geophysics and Volcanology, and numerous local organizations (see Van der Lee et al. (2001)). We thank the many individuals associated with MIDSEA (see Van der Lee et al. (2001)); their support has been invaluable. Data for PAB (GSN), MAHO (Geofon), and VSL, KEG and MDT (all MedNet) were obtained from the ORFEUS Data Center, the GEOFON Data Center, and the IRIS DMC, respectively. We greatly appreciate regular and valuable discussions with F. Marone and C. Schmid. We are very grateful to M. Flanagan, G. Helffrich, and H. Paulssen, for insightful comments on this study and thorough, constructive reviews, which helped to significantly improve the manuscript.

References

Akaogi, M., Ito, E., Navrotsky, A., 1989. Olivine-modified spinel-spinel transitions in the system Mg_2SiO_4-Fe_2SiO_4: calorimetric measurements, thermochemical calculation, and geophysical application. J. Geophys. Res. 94, 15671–15685.

Aki, K., Richards, P., 2002. Quantitative Seismology, second ed. University Science Books.

Ammon, C., 1991. The isolation of receiver effects from teleseismic P waveforms. Bull. Seism. Soc. Am. 81, 2504–2510.

Benz, H., Vidale, J., 1993. Sharpness of upper mantle discontinuities determined from high-frequency reflections. Nature 365, 147–150.

Bina, C., Helffrich, G., 1994. Phase transition Clapeyron slopes and transition zone seismic discontinuity topography. J. Geophys. Res. 99 (B8), 15853–15860.

Bina, C., Wood, B., 1987. The olivine-spinel transitions: Experimental and thermodynamic constraints and implications for the

nature of the 400-km seismic discontinuity. J. Geophys. Res. 92, 4853–4866.

Cammarano, F., Goes, S., Vacher, P., Giardini, D., 2003. Inferring upper mantle temperatures from seismic velocities. Phys. Earth Planet. Inter. 138 (3–4), 197–222.

Castle, J., Van der Hilst, R., 2003. Searching for seismic scattering off mantle interfaces between 800 km and 2000 km depth. J. Geophys. Res. 108 (B2), 2095.

Chevrot, S., Vinnik, L., Montagner, J.-P., 1999. Global-scale analysis of the mantle Pds phases. J. Geophys. Res. 104 (B9), 20203–20219.

Collier, J., Helffrich, G., 1997. Topography of the "410" and "660" km discontinuities in the Izu-Bonin subduction zone. Geophys. Res. Lett. 24, 1535–1538.

Collier, J., Helffrich, G., Wood, B., 2001. Seismic discontinuities and subduction zones. Phys. Earth Planet. Inter. 127, 35–49.

Cummins, P., Kennett, B., Bowman, J., Bostock, M., 1992. The 520 km discontinuity. Bull. Seismol. Soc. Am. 82, 323–336.

Deuss, A., Woodhouse, J., 2001. Seismic observations of splitting of the mid-transition zone discontinuity in Earth's mantle. Science 294, 354–357.

Deuss, A., Woodhouse, J., 2002. A systematic search for mantle discontinuities using SS-precursors. Geophys. Res. Lett. 29 (8), 10.1029/2002GL014768.

Dueker, K., Sheehan, A., 1998. Mantle discontinuity structure beneath the colorado rocky mountains and high plains. J. Geophys. Res. 103, 7153–7169.

Dziewonski, A., Anderson, D.L., 1981. Preliminary reference Earth model. Phys. Earth Planet. Inter. 25, 297–356.

Estabrook, C., Kind, R., 1996. The nature of the 660-kilometer upper-mantle siesmic discontinuity from precursors to the PP phase. Science 274, 1179.

Faccenna, C., Jolivet, L., Piromallo, C., Morelli, A., 2003. Subdusction and the depth of convection in the mediterranean mantle. J. Geophys. Res. 180 (B2), 2099, doi:10.1029/2001JB001690.

Flanagan, M., Shearer, P., 1998. Global mapping of topography on transition zone velocity discontinuities by stacking SS precursors. J. Geophys. Res 103, 2673–2692.

Gossler, J., Kind, R., 1996. Seismic evidence for very deep roots of continents. Earth Planet. Sci. Lett. 138, 1–13.

Gu, Y., Dziewonski, A., 2002. Global variability of transition zone thickness. J. Geophys. Res. 107 (7), doi:10.1029/2001JB000489.

Gu, Y., Dziewonski, A., Agee, C., 1998. Global de-correlation of the topography of transition zone discontinuities. Earth Planet. Sci. Lett. 157, 57–67.

Gurrola, H., Minster, J., Owens, T., 1994. The use of velocity spectrum for stacking receiver functions and imaging upper mantle discontinuities. Geophys. J. Int. 117, 427–440.

Hanka, W., Li, X., Davila, J., Pazos, A., Bock, G., Kind, R., 2001. Investigation of the crust and upper mantle in the western Mediterranean. In: Eos. Trans. AGU. AGU 2001 Fall Meeting, vol. 82, San Francisco. 910.

Helffrich, G., 2000. Topography of the transition zone seismic discontinuities. Rev. Geophys. 38 (1), 141–158.

Helffrich, G., Asencio, E., Knapp, J., Owens, T. J., 2003. Transition zone structure in a tectonically inactive area: 410 and 660 km discontinuity properties under the northern North Sea. Geophys. J. Int. 155, 193–199.

Helffrich, G., Bina, C., 1994. Frequency dependence of the visibility and depths of mantle seismic discontinuities. Geophys. Res. Lett. 21 (24), 2613–2616.

Helffrich, G., Wood, B., 1996. 410-km discontinuity sharpness and the form of the olivine α-β phase diagram: resolution of apparent seismic contradictions. Geophys. J. Int. 126, F7–F12.

Higo, Y., Inoue, T., Irifune, T., Yurimoto, H., 2001. Effect of water on the spinel-postspinel transformation in Mg_2SiO_4. Geophys. Res. Lett. 28 (18), 3505–3508.

Inoue, T., Weidner, D., Northrup, P., Parise, J., 1998. Elastic properties of hydrous ringwoodite (γ-phase) in Mg_2SiO_4. Earth Planet. Sci. Lett. 160, 107–113.

Ita, J., Stixrude, L., 1992. Petrology, elasticity, and composition of the mantle transition zone. J. Geophys. Res 97, 6849–6866.

Ito, E., Takahashi, E., 1989. Postspinel transformations in the system Mg_2SiO_4-Fe_2SiO_4 and some geophysical implications. J. Geophys. Res. 94 (B8), 10637–10646.

Jones, L., Mori, J., Helmberger, D., 1992. Short-period constraints on the proposed transition zone discontinuity. J. Geophys. Res. 97, 8765–8774.

Karato, S., 2003. The Dynamic Structure of the Deep Earth. Princeton University Press, Princeton.

Karato, S., Ohtani, E., 1992. Interior structure of the Earth. In: Stacey, F. (Ed.), Physics of the Earth. Brookfield Press, Brisbane, Australia, pp. 127–148.

Katsura, T., Ito, E., 1989. The system Mg_2SiO_4-Fe_2SiO_4 at high pressures and temperatures: Precise determination of stabilities of olivine, modified spinel, and spinel. J. Geophys. Res. 94, 15663–15670.

Kawakatsu, H., Niu, F., 1994. Seismic evidence for a 920-km discontinuity in the mantle. Nature 371, 301–305.

Kennett, B., Engdahl, E., 1991. Traveltimes for global earthquake location and phase identification. Geophys. J. Int. 105, 429–465.

Kennett, B., Engdahl, E., Buland, R., 1995. Constraints on seismic velocities in the earth from traveltimes. Geophys. J. Int. 122, 108–124.

Koito, S., Akaogi, M., Kubota, O., Suzuki, T., 1996. Calorimetric measurements of perovskites in the system $CaTiO_3$-$CaSiO_3$ and experimental and calculated phase equilibria for high-pressure dissociation of diopside. Phys. Earth Planet. Inter. 123, 345–357.

Langston, C., 1979. Structure under Mount Rainier, Washington, inferred from teleseismic body waves. J. Geophys. Res. 84, 4749–4762.

Le Stunff, Y., Wicks, C., Romanowicz, B., 1995. P′P′ precursors under Africa: evidence for mid-mantle reflectors. Science 270, 74–77.

Lebedev, S., Chevrot, S., van der Hilst, R., 2002. The 660-km discontinuity within the subducting nw-pacific lithospheric slab. Earth Planet. Sci. Lett. 205, 25–35.

Leven, J., 1985. The application of synthetic seismograms to the interpretation of the upper mantle P-wave velocity structure in northern Australia. Phys. Earth Planet. Inter. 38, 9–27.

Li, A., Fischer, K., Van der Lee, S., Wysession, M., 2002. Crust and upper mantle discontinuity structure beneath eastern North America. J. Geophys. Res. 107 (B5), 10.1029/2001JB000190.

Li, B., Liebermann, R., Weidner, D., 2001. P-V-V_p-V_s-T measurements on wadsleyite to 7 GPa and 873 k: implications for the 410-km discontinuity. J. Geophys. Res. 106 (B12), 30575–30591.

Li, X., Bock, G., Vafidis, A., Kind, R., Harjes, H.-P., Hanka, W., Wylegalla, K., Van der Meijde, M., Yuan, X., 2003. Receiver function study of the Hellenic subduction zone: imaging crystal thickness variations and the oceanic Moho of the descending African lithosphere. Geophys. J. Int. 155, 733–748.

Li, X., Kind, R., Yuan, X., Sobolev, S., Hanka, W., Ramesh, D., Gu, Y., Dziewonski, A., 2003. Seismic observtion of narrow plumes in the oceanic upper mantle. Geophys. Res. Lett. 30, doi:10.1029/2002GL015411.

Marone, F., van der Lee, S., Giardini, D., 2004. 3d upper mantle s-velocity model for the Eurasia-Africa plate boundary region. Geophys. J. int. 158, 109–130.

Marone, F., Van der Meijde, M., Van der Lee, S., Giardini, D., 2003. Joint inversion of local, regional and tele seismic data for crystal thickness in the Eurasia-Africa plate boundary region. Geophys. J. Int. 154, 499–514.

Montelli, R., Nolet, G., Dahlen, F., Masters, G., Egdahl, E., Hung, S., 1999. Finite-frequency tomography reveals a variety of plumes in the mantle. Tectonophysics 314, 373–385.

Morelli, A., Dziewonski, A., 1993. Body wave traveltimes and a spherically symmetric P- and S-wave velocity model. Geophys. J. Int. 112, 178–194.

Morelli, A., Piromallo, C., 2000. The late stage of retreating subduction in the Alpine-Mediterranean region: constraints from travel time seismic tomography. In: Boschi, E., Ekström, G., Morelli, A. (Eds.), Problems in Geophysics for the New Millennium. Editrice Compositori, Bologna, pp. 179–215.

Neele, F., de Regt, H., VanDecar, J., 1997. Gross errors in upper-mantle discontinuity topography from underside reflection data. Geophys. J. Int. 129 (1), 194–204.

Niu, F., Kawakatsu, H., 1995. Direct evidence for the undulation of the 660-km discontinuity beneath Tonga: Comparison of Japan and California array data. Geophys. Res. Lett. 22, 531–534.

Niu, F., Kawakatsu, H., 1997. Depth variation of the mid-mantle seismic discontinuity. Geophys. Res. Lett. 24, 429–432.

Olivieri, M., Morelli, A., 2001. The transition zone in the Mediterranean region: new constraints from P to S conversions. Eur. Geophys. Soc. Newslett. 78, 49.

Owens, T., Zandt, G., Taylor, S., 1984. Seismic evidence for an ancient rift beneath the Cumberland Plateau, Tennessee: a detailed analysis of broadband teleseismic P waveforms. Bull. Seism. Soc. Am. 77, 7783–7795.

Paulssen, H., 1988. Evidence for a sharp 670-km discontinuity as inferred from p-to-s converted waves. J. Geophys. Res. 93 (B9), 10489–10500.

Paulssen, H., 1988. Evidence for small scale structure of the upper mantle. Ph.D. thesis, Utrecht University.

Petersen, N., Vinnik, L., Kosarev, G., Kind, R., Oreshin, S., Stammler, K., 1993. Sharpness of the mantle discontinuities. Geophys. Res. Lett. 20, 859–862.

Piromallo, C., Morelli, A., 2003. P wave tomography of the mantle under the Alpine-Mediterranean area. J. Geophys. Res. 108 (B2), 2065, doi:10.1029/2002JB001757.

Revenaugh, J., 1990. Reflectivity of the transition zone: constraints on the 530-km discontinuity from ScS reverberations. EOS 17, 1472.

Revenaugh, J., Jordan, T., 1991. Mantle layering from ScS reverberations: 2. The transition zone. J. Geophys. Res. 96, 19763–19780.

Richards, M., Wicks, C., 1990. S-P conversion from the transition zone beneath Tonga and the nature of the 670 km discontinuity. Geophys. J. Int. 101 (1), 1–35.

Rigden, S., Gwanmesia, G., Fitzgerald, J., Jackson, I., Liebermann, R., 1991. Spinel elasticity and seismic structure of the transition zone of the mantle. Nature 354, 143–145.

Ringwood, A., 1975. Composition and Petrology of the Earth's Mantle. McGraw-Hill, New York, p. 618.

Schmid, C., van der Lee, S., Giardini, D., 2004. Delay times and shear wave splitting in the Mediterranean region. Geophys. J. Int. 159 (1), 275–290.

Shearer, P., 1990. Seismic imaging of upper-mantle structure with new evidence for a 520-km discontinuity. Nature 344, 121–126.

Shearer, P., 1991. Constraints on upper mantle discontinuities from observations of long-period ss precursors. J. Geophys. Res. 96 (18), 18147–18182.

Shearer, P., 2000. Upper mantle seismic discontinuities. Geophys. Monogr. 117, 115–131.

Shearer, P., Flanagan, M., 1999. Seismic velocity and density jump across the 410- and 660-km discontinuities in Earth's upper mantle. Science 285, 1545–1548.

Smyth, J., Frost, D., 2002. The effect of water on the 410-km discontinuity: an experimental study. Geophys. Res. Lett. 29 (10), 10.1029/2001GL014418.

Smyth, J., Kawamoto, T., 1997. Wadsleyite II: a new high pressure hydrous phase in the peridotite-H_2O system. Earth Planet. Sci. Lett. 146, E9–E16.

Van der Lee, S., Marone, F., Van der Meijde, M., Giardini, D., Deschamps, A., Margheriti, L., Burkett, P., Solomon, S., Alves, P., Chouliaras, M., Eshwehdi, A., Suleiman, A., Gashut, H., Herak, M., Ortiz, R., Davila, J., Ugalde, A., Vila, J., Yelles, K., 2001. Eurasia-Africa plate boundary region yields new seismographic data. Eos 82, 637–646.

Van der Lee, S., Paulssen, H., Nolet, G., 1994. Variability of p660s phases as a consequence of topography of the 660-km discontinuity. Phys. Earth Planet. Int. 86, 147–164.

Van der Meijde, M., Marone, F., Van der Lee, S., Giardini, D., 2003. Seismic evidence for water deep in Earth's upper mantle. Science 300, 1556–1558.

Van der Meijde, M., Van der Lee, S., Giardini, D., 2003. Crystal structure beneath broadband seismic stations in the Mediterranean region. Geophys. J. Int. 152 (3), 729–739.

Vidale, J., Benz, H., 1992. Upper-mantle seismic discontinuities and the thermal structure of subduction zones. Nature 356, 678–683.

Vidale, J., Ding, X.-Y., Grand, S., 1995. The 410-km-depth discontinuity: a sharpness estimate from near-critical reflections. Geophys. Res. Lett. 22, 2557–2560.

Vinnik, L., Kato, M., Kawakatsu, H., 2001. Search for seismic discontinuities in the lower mantle. Geophys. J. Int. 147, 41–56.

Wang, Y., Guyot, F., Lieberman, R., 1992. Electron microscopy of (Mg, Fe)SiO (sub 3) perovskite; evidence for structural phase

transitions and implications for the lower mantle. J. Geophys. Res. 97 (9), 12327–12347.

Wood, B., 1990. Postspinel transformations and the width of the 670-km discontinuity: a comment on "Postspinel transformations in the system Mg_2SiO_4-Fe_2SiO_4 and some geophysical implications" by E. Ito and E. Takahashi. J. Geophys. Res. 95 (B8), 12681–12688.

Wood, B., 1995. The effect of H_2O on the 410-kilometer seismic discontinuity. Science 268, 74–76.

Woodland, A., 1998. The orthorhombic to high-*p* monoclinic phase transition in Mg-Fe pyroxenes: can it produce a seismic discontinuity. Geophys. Res. Lett. 25 (8), 1241–1244.

Wortel, M., Spakman, W., 2000. Subduction and slab detachment in the Mediterranean-Carpathian region. Science 290, 1910–1917.

Yamazaki, A., Hirahara, K., 1994. The thickness of upper mantle discontinuities, as inferred from short-period J-array data. Geophys. Res. Lett. 21 (17), 1811–1814.